Title

Use of a GPS-Derived Troposphere Model to Improve InSAR Deformation Estimates in the San Gabriel Valley, California

Journal

IEEE Transactions on Geoscience and Remote Sensing, 54(9)

ISSN

0196-2892

Authors

Houlié, Nicolas
Funning, Gareth J
Bürgmann, Roland

Publication Date

2016-09-01

DOI

10.1109/tgrs.2016.2561971

Peer reviewed

Use of a GPS-Derived Troposphere Model to Improve InSAR Deformation Estimates in the San Gabriel Valley, California

Nicolas Houlié, Gareth J. Funning, and Roland Bürgmann

This work was supported in part by Southern California Earthquake Center under Award 08126. The work of N. Houlié was supported in part by the U.S. Geological Survey under Cooperative Agreement 07HQAG0031 and in part by the University of California at Berkeley. The work of G. J. Funning was supported in part by the Department of Energy and in part by a Lindemann Trust Postdoctoral Fellowship. The authors declare no competing financial interests. This research was supported by the Southern California Earthquake Center (Contribution No. 6263). SCEC is funded by NSF Cooperative Agreement EAR-1033462 & USGS Cooperative Agreement G12AC20038. http://www. scec.org/publication/6263.

This paper has supplementary downloadable material available at http:// ieeexplore.ieee.org, provided by the authors.

N. Houlié is with the Mathematical and Physical Geodesy Group, Institute of Geodesy and Photogrammetry, and also with the Seismology and Geodynamics Group, Institute of Geophysics, ETH Zurich, 8093 Zurich, Switzerland (e-mail: nhoulie@ethz.ch). G. J. Funning is with the Department of Earth Sciences, University of California at Riverside, Riverside, CA 92521 USA. R. Bürgmann is with the Berkeley Seismological Laboratory, University of California at Berkeley, Berkeley, CA 94720 USA.

Abstract:

We evaluate the potential of troposphere models derived from ground meteorological data (pressure, temperature, and relative humidity) and Global Positioning System (GPS) data to improve InSAR measurements and models derived from them. We test this approach on an ERS-2/Envisat data set collected during a transient surface deformation episode that occurred from January to July 2005 in the San Gabriel Valley, southern California, USA. We find that the interferometric phase change observed over the corresponding period cannot be solely attributed to hydrological uplift associated with rising groundwater levels but also includes a significant contribution from differential tropospheric delay due to differing quantities of water vapor in the troposphere on the two SAR observation dates. We show that, if the tropospheric phase contribution is mistakenly interpreted as the range change associated with changes in groundwater storage, both the surface displacement and the groundwater storage coefficient may be overestimated by up to 30%. This method could be applied in real time where meteorological measurements are available near one or more GPS permanent site(s).

Index Terms—Geodesy, global positioning system (GPS), interferometric synthetic aperture radar (InSAR), seismology, tectonics, troposphere.

SECTION I.

Introduction

The Global Positioning System (GPS) and interferometric synthetic aperture radar (InSAR) are commonly used to estimate surface deformation. The two techniques are highly complementary, i.e., GPS is particularly sensitive to horizontal motions, whereas InSAR, although somewhat sensitive to E–W motions, is mostly sensitive to those in the vertical direction. GPS, when operated in continuous mode (C-GPS), has good resolution in time (up to 50 Hz), but, because high operating costs limit the density of networks, regional networks are typically composed of a site every 15–30 km. On the other hand, InSAR provides a spatially dense set of measurements, with a resolution < 100 m, but its temporal resolution, which is limited by the return period of the satellite being used, is on the order of days to months. By combining both data types together in joint studies, the 3-D surface displacement field allows the characterization of multiple deformation types, including hydrologic and anthropogenic deformation [1]–[2][3], surface mass movements [4]–[5][6], volcanic [8]–[9][10][11][12][13][14], and tectonic processes [15]–[16][17]. Sometimes, the amplitudes of specific deformation features, e.g., interseismic [18]–[19][20] and postseismic deformation [21], are small enough that they could be masked by the signals associated with changes in the troposphere state between observation epochs.

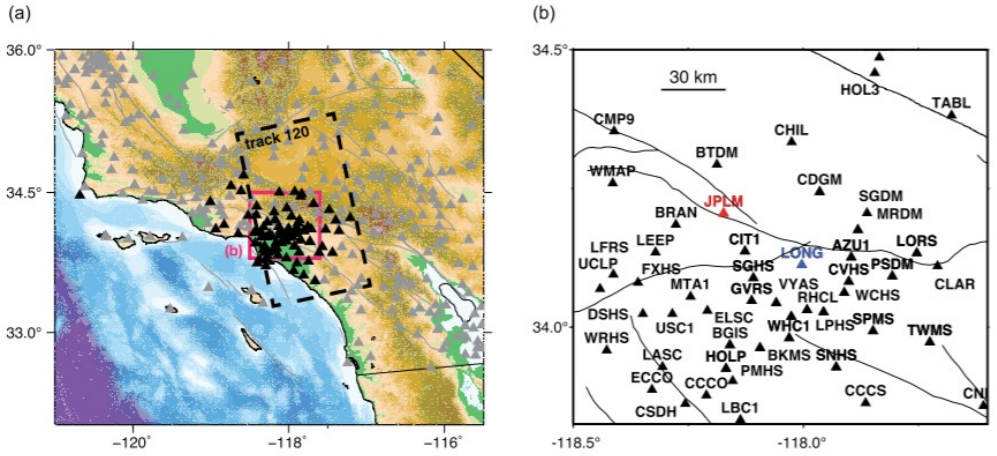

Fig. 1. Location of the study area. (a) Map of the southern California region, showing (gray triangles) present-day Plate Boundary Observatory (PBO) C-GPS stations and (black triangles) the SCIGN stations available in 2005 that are used in this study. Pink box shows area of the greater Los Angeles area that is the focus of this study. Black frame indicates the area covered by the Envisat track 120 interferogram shown in Fig. 2. (b) Map of the GPS stations in the greater Los Angeles area used in this study. Meteorological data (pressure, temperature, and relative humidity) were available at the JPL site (JPLM). The maximum displacement from the 2005 uplift event is located beneath the site LONG.

While their resolutions are different, both InSAR and GPS are adversely affected by the troposphere water vapor content (WVC) at the time of an observation. The WVC in the troposphere refracts and delays the microwave signals transmitted by a GPS or InSAR satellite on their paths to receivers/ground reflectors. During the processing of GPS data, a 1-D troposphere model is used to estimate a troposphere delay (TD) correction and thus correct, through time, the signal phases received from various

satellites. Unlike in GPS processing, the atmosphere phase screen remains difficult to remove automatically in standard InSAR processing [22], although some progress has been made in recent years [22], [23]. Any difference in the spatial pattern of tropospheric state between the two acquisition epochs is overprinted upon any surface displacement and/or topographic signals in the data. In the rare but optimum case that the TD changes are constant over the interferogram, the troposphere would remain invisible to InSAR, as only spatial changes in the interferometric phase can be identified. More typically, some parts of the scenes are more severely impacted by WVC differences than others, which can lead to surface deformation being masked or its pattern changed in interferograms. If sufficient numbers of independent interferograms spanning a deformation episode can be formed, the effects of tropospheric variations can be mitigated by stacking [24]–[25] [26], albeit at the loss of time-dependent information, or by spatiotemporal filtering of the time series data [27]–[28][29][30]. However, the usefulness of a single interferogram, and therefore the opportunity to quickly and robustly image rapid changes or precursory effects (for instance, a notional aseismic slip precursor to an earthquake), can often be limited by tropospheric state changes.

The challenge of understanding the contribution of tropospheric water vapor to the observed signal led to a series of studies of the troposphere using GPS [31]–[32][33][34][35][36][37][38][39][40][41][42][43][44], InSAR alone [22], [45]–[46][47][48][49] or both combined with long-wavelength meteorological models [50]–[51][52][53][54] or other satellite observations such as MODIS or MERIS [55]–[56][57][58]. The great diversity of approaches is well founded since understanding troposphere complexity is made easier when auxiliary data sets (e.g., topography, GPS, and multispectral imagery) are available because InSAR and GPS scan the troposphere in different ways. InSAR is only sensitive to the troposphere over a path in a single direction: that of the line of sight (LOS) between the satellite platform and the ground target. Any wave propagation delay due to tropospheric effects is accumulated over that whole path, meaning that variations in water vapor density in the LOS cannot be isolated *a priori*. The GPS system, on the other hand, does not scan solely in one LOS direction. Instead, each GPS receiver on the ground tracks continuously changes in carrier signal phase for between 5 and 12+ satellites, in LOS directions that vary over time as the satellites move across the sky. For a sky visibility of 15° above the horizon, one GPS site can be continuously scanning approximately 30 km of the surrounding troposphere. Given a mean station spacing that is less than this radius, any tropospheric delay is therefore correlated over the network, and the redundancy in the data can be used to estimate the tropospheric delay at each station. Dense GPS networks, therefore, have the potential to map tropospheric WVC in both space and time. Given that the troposphere is not dispersive with respect to microwave radiation, GPS-derived troposphere models can theoretically be used to correct for the troposphere contribution to a SAR

interferogram, although different microwave frequencies are used between the two methods [44], [59]–[60][61].

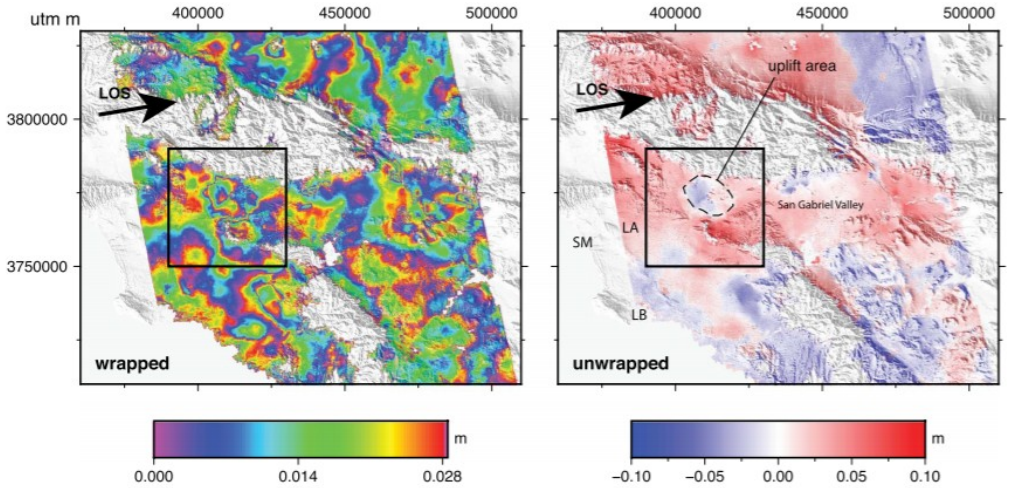

Fig. 2. Wrapped and unwrapped interferograms of the study area spanning the 2005 uplift event. Data are from Envisat (track 120) acquisition dates 2005/01/26 and 2005/07/20 (see Table I), and these have been converted to the LOS displacement equivalent. Negative LOS displacements are decreases in range to the satellite (consistent with uplift of the ground), and vice versa. The black box indicates the area shown in Fig. 6. LA, LB, and SM stand for Los Angeles, Long Beach, and Santa Monica, respectively.

TABLE I
DETAILS OF SAR IMAGES PROCESSED. BASELINES AND ALTITUDE OF AMBIGUITIES ARE GIVEN AT THE CENTER OF THE IMAGE. LETTERS A AND D IN COLUMN 2 STAND FOR ASCENDING AND DESCENDING TRACKS

Satellite	Track	Date 1	Date 2	Time interval (days)	Perp. baseline (m)	‖ Altitude of ambiguity ‖ (m)	Figure
ENVISAT	120A	26-Jan-2005	20-Jul-2005	175	39	241	2 and A2
ENVISAT	120A	26-Jan-2005	11-May-2005	105	251	40	A2
ENVISAT	120A	11-May-2005	20-Jul-2005	70	-212	48	A2
ENVISAT	170D	29-Jan-2005	14-May-2005	105	-558	18	A4
ENVISAT	170D	29-Jan-2005	23-Jul-2005	175	-590	17	A4
ENVISAT	170D	14-May-2005	23-Jul-2005	70	-32	312	A4
ERS-2	442D	13-Jan-2005	24-Mar-2005	70	310	32	A6
ERS-2	442D	28-Apr-2005	2-Jun-2005	35	177	57	A6
ERS-2	442D	28-Apr-2005	11-Aug.2005	105	225	44	A6
ERS-2	170D	29-Jan-2005	5-Mar-2005	35	45	225	A8
ERS-2	170D	29-Jan-2005	14-May-2005	105	234	43	A8
ERS-2	170D	29-Jan-2005	23-Jul-2005	175	201	50	A8
ERS-2	170D	5-Mar-2005	14-May-2005	70	116	86	A10
ERS-2	170D	5-Mar-2005	23-Jul-2005	141	70	143	A10
ERS-2	170D	14-May-2005	23-Jul-2005	70	-32	305	A10

To build a satisfactory model of the tropospheric delay using GPS data, the troposphere state must be stable enough (< 2 h) to permit an accurate estimation of tropospheric delay around each GPS antenna. Where it is available, meteorological information collected on the ground may allow us to assess this stability. More importantly, if surface meteorological sensors are collocated with C-GPS sites, their data can then be used to calibrate the static portion of the troposphere model at the surface and thus reduce the uncertainty in our TD estimates. As meteorological and GPS data are

nowadays available in real time, we believe that TDs could be generated in near real-time (i.e., every hour, and/or at times of SAR satellite overflight).

The aim of this study is to test whether ground meteorological measurements can enable the robust mitigation of tropospheric water vapor signals in InSAR data spanning a deformation event. We use GPS data collected by the Southern California Integrated GPS Network (SCIGN; see Fig. 1), a dense array of continuously recording stations in the greater Los Angeles area (LA; see Fig. 2). Specifically, we focus on an uplift event that occurred in the San Gabriel Valley, which is approximately 30 km northeast of LA, in early 2005. Up to 6 cm of vertical displacement, affecting seven SCIGN permanent GPS sites, was detected by both GPS and InSAR monitoring [62]. This 15-km-wide uplift feature was interpreted as a hydrogeological response to high rainfall in the spring of 2005, based on the similarities between GPS, groundwater well levels, and InSAR measurements during the rainfall episodes of the year 2005. Here, we assess the effects and potential data improvements that arise from the integration of meteorological data into our GPS processing and, hence, the component of the InSAR signal that has a tropospheric origin. We also integrate surface meteorological data, i.e., pressure (P), temperature (T), and relative humidity (H), collected by the Jet Propulsion Laboratory (JPL) near a C-GPS station (site JPLM) into our processing, and assess its impact on both our tropospheric delay models and station coordinate estimates.

SECTION II.

SAR Analysis

We process 15 pairs of ERS-2 and Envisat ASAR images (see Table I) using the ROI_PAC software [63], and the 1-arc-second digital elevation model (DEM) generated by the Shuttle Radar Topography Mission (SRTM). For clarity purposes, we show hereinafter only the results associated with one Envisat pair (track 120, 26.01.2005–20.07.2005). The altitude of ambiguity of this image pair (241 m) is greatly in excess of the < 10-m elevation uncertainty in the SRTM DEM [64], suggesting that topographic errors or satellite artifacts [65] will not contribute significantly to the processed differential interferogram. Delft precise orbits [66] were used to correct for orbital phase differences. Regarding post-interferogram formation, a power spectrum filter [67] was applied, and the data were unwrapped using a branch-cut unwrapper [68]. The interferogram that we obtain is shown in Fig. 2, with the phase change converted into LOS displacement. The signal is very heterogeneous, with several prominent regions ~10–20 km across showing amplitudes equivalent to 3–5 cm of apparent surface displacement with respect to more stable areas, such as downtown Los Angeles.

At least two of these large interferogram signals are correlated with known aquifers, i.e., the target uplift signal in the San Gabriel Valley, in the northwest of the image, and a subsidence signal located in the Santa Ana basin ~45 km further to the south southeast, as observed in previous InSAR

investigations of the greater Los Angeles area [15], [16]. Other spatially correlated features of a similar scale/shape are not easily attributed to known deformation sources; however, a region of large apparent subsidence ~15 km to the SSE of the San Gabriel Valley, which is close to, but does not entirely match, the location of an approximately linear band of oil fields [16], i.e., an area of apparent uplift 10 km NE of the Santa Ana aquifer, is even harder to attribute to a known source, since it does not coincide with either oil wells or mapped aquifers. In addition to the larger scale “blobs”, numerous smaller features (i.e., wavelengths of a few kilometers) can also be distinguished in the data, only a few of which can be attributed to known areas of subsidence due to oil or water extraction [16]. This complex pattern of change may be explained by the proximity of the ocean, which induces a heterogeneous distribution of tropospheric water vapor in the atmosphere.

We note that our InSAR range-change data may also contain signals correlated with the topography. In our experience, however, any such correlation will not be uniform in space, or be satisfactorily removed using a simple linear relationship between interferometric phase and altitude [69]. In some areas, particularly those with high relief, characteristic length scales of tropospheric noise have been identified in the InSAR time series and successfully used to generate transfer functions for removing topographically correlated noise [46]. This style of correction is not infallible; however, similar methods have been shown to work even when the topographic data were taken from a different region [70], and in areas where the topography is locally flat, such as the center of the San Gabriel Valley, tropospheric signals on small spatial scales cannot be correlated with surface elevation. We also note that topography correlation corrections may also remove real tectonic deformation if the signal is correlated with the topography [71]. Therefore, by integrating estimates of tropospheric delay from the GPS data, we attempt to provide a significant improvement to the surface deformation signal in the target area of our interferogram over altitude-only-based corrections.

SECTION III.

GPS Analysis

We process the GPS data recorded from 2004 to 2006 at 46 SCIGN permanent GPS stations in southern California using the GAMIT processing software [72] within the International Terrestrial Reference Frame 2000 [73] to anchor the local network solutions into a stable reference frame. We have chosen to estimate 13 TDs per day using the Saastamoinen atmospheric model [74], corresponding to a regular estimate of troposphere state every 2 h, plus an additional estimate at the time of flyover of the Envisat satellite on the days of ascending track image acquisition (approximately 05:40 UTC). We have used a minimum elevation angle for station–satellite pairs of 15° above the horizon. This means, assuming that the tropospheric delay is dominantly from the water vapor below 4-km elevation [31], every GPS

antenna is affected by the troposphere state within a ~30-km radius. As the average station separation of the network is ~5–10 km, this permits a robust estimate of the first-order spatial variation in tropospheric delay in the Los Angeles (LA) area. The TD is modeled in GPS processing software packages as a function of elevation and azimuth and integrated along a ray path (*dS*), i.e.,

$$TD = \int N dS \qquad (1)$$

where *N*, i.e., the refractivity of the atmosphere, can be decomposed, as follows, into hydrostatic and wet TDs:

$$TD = TD_{\text{dry}}(P, T) + TD_{\text{wet}}(e, T) \qquad (2)$$

with

$$N = N_{\text{dry}} + N_{\text{wet}} \qquad (3)$$

$$N = k_1 \frac{P}{T} + \left((k_2 - k_1) \frac{e}{T} + k_3 \frac{e}{T^2} \right). \qquad (4)$$

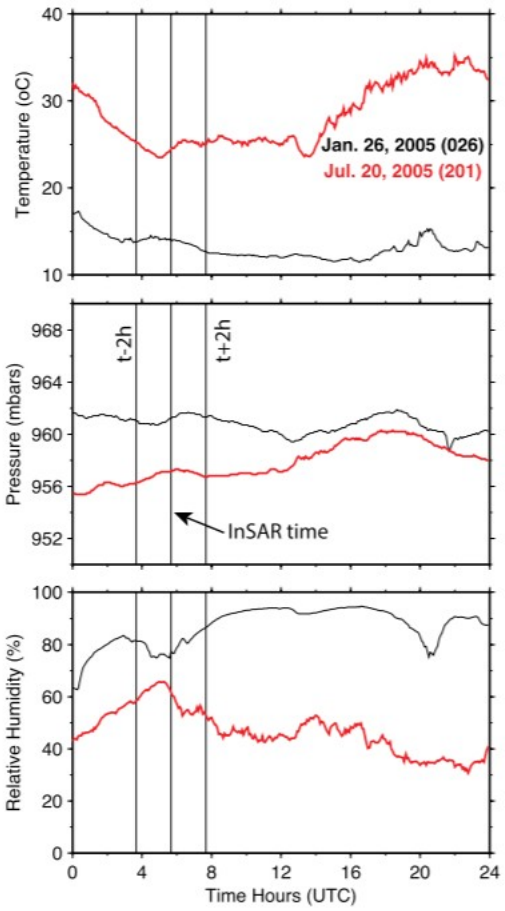

Fig. 3. (Top) Daily temperature (T), (middle) pressure (P), and (bottom) relative humidity (H) time series at the JPLM C-GPS/meteorological site corresponding to (black) January 26 and (red) July 20, 2005. Three vertical lines are plotted: the middle line indicates the SAR acquisition time; the other two delimit the start and end of the time 4-h window of the GPS data used to estimate the tropospheric delay. Around the SAR acquisition time, we observe that all parameters are stable (i.e., $dT \sim \pm 2$ K, $dP \sim 1$ mbar, and $dH \pm 10\%$). Therefore, we assume that GPS measurements combined with surface meteorological parameters allows a robust estimation of the TD.

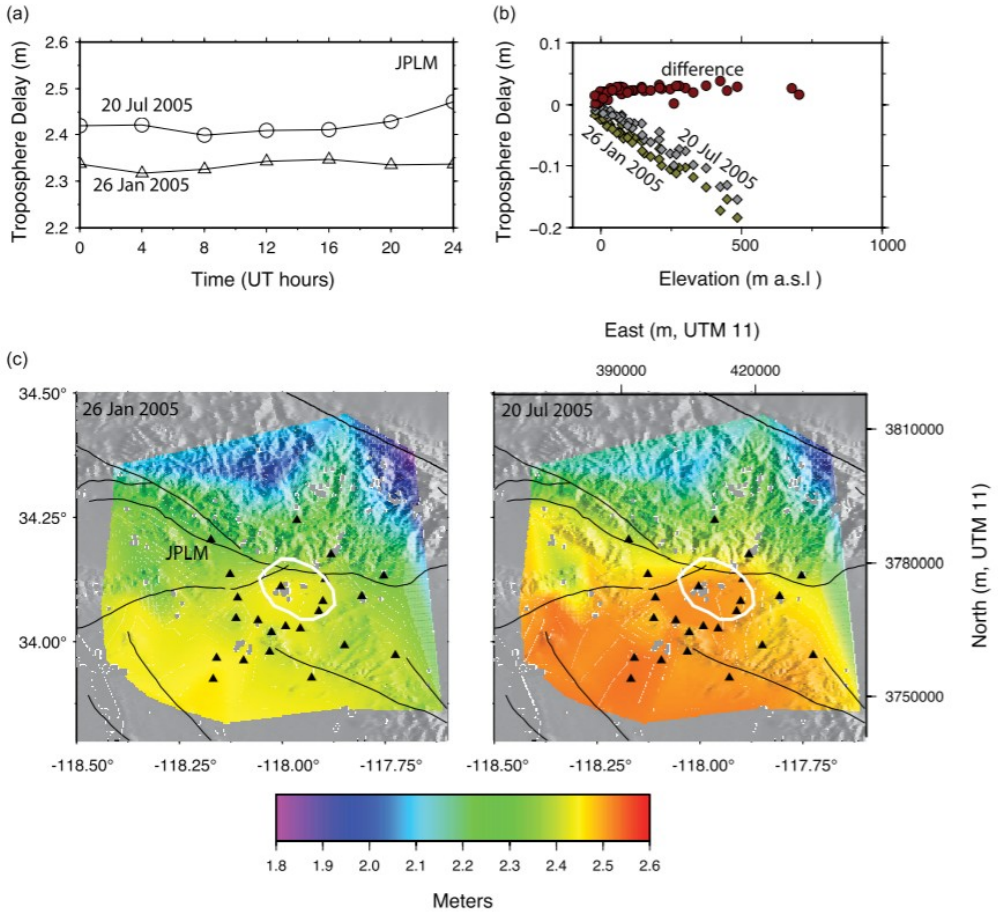

Fig. 4. Example estimates of ZTD. (a) Troposphere zenithal delay of the two days of SAR image acquisitions at GPS site JPLM. The TD does not vary dramatically on the two days, although a systematic TD difference is observed between the two days of sampling. The TD variations is $\sim 8.8 \pm 2.5$ cm. (b) Relationship of TD with elevation above sea level. (c) Spatially interpolated patterns of TD for the times of acquisition of the two SAR images.

Here, e is the partial water vapor pressure (in hectopascals), T is the temperature (in kelvin), P is the total pressure (in hectopascals), and k_1, k_2, k_3 are the three empirical constants (i.e., k_1=77.60±0.009 K/hPa, k_2=69.4±2.2 K/hPa, k_3=370100±1200 K/hPa) [75]. In a stratified atmosphere, T and P can be approximated as functions of the altitude z (m) only, i.e.,

$$T = T_{(z=0)} - 0.006\, z \qquad (5)$$

and after Triplet and Roche (1983), i.e.,

$$P = P_{(z=0)} \left[1 - \frac{6.5\ 10^{-3} z}{288.15} \right]^{5.256}. \qquad (6)$$

The TD is then estimated in various directions using GPS data and converted into zenithal TD (ZTD) using a mapping function [74]. Partial water vapor pressure e, however, not only is a linear function of altitude but also depends on the averaged air temperature and of some local settings, such as water

storage, wind conditions, and topography. We estimate the contribution of e on the wet and total TD [see (1) and (2)] using an empirical relationship derived using Global Positioning System (GPS), Détermination d'Orbite et Radiopositionnement Intégré par Satellite (DORIS), and radiosonde data [31]. Effectively, in most cases, wet TD does not exceed 30 cm (or 25% of the total TD for the lowest elevation angles). This 1-D model is efficient enough to correctly estimate the TD generated by a “smooth” troposphere (i.e., the delay varies with a wavelength significantly larger than the GPS station spacing in southern California). However, a 1-D model of the troposphere state is not able to reflect any potential heterogeneous effect of the troposphere on the data sets. Estimation of the 3-D distribution of water vapor in the troposphere, which would be necessary to resolve any such heterogeneity, is currently, we believe, beyond the capabilities of the SCIGN network. Indeed, to detect such heterogeneities, a densification of the network may be required to be upgraded to < 2-km station spacing.

After we first process the data using the standard meteorological conditions (i.e., T=273 K, P=1 bar, and H=50%), we could define that the stability of the TDs were stable during the SAR image acquisition days (see Fig. 4). Average TDs for both days differ of ~10 cm and of ~5 cm within each day. In the second phase, we include the meteorological data recorded at JPLM in the GPS data processing. We specify $P(z=0)$, $T(z=0)$, and H (constant through the column) parameters at the surface and constrain the ZTD to be bounded by ±5 cm from the state defined by ground measurements (1-sigma interval, i.e., the width of this interval has been determined by the processing of GPS data with standard atmosphere modeling), reflecting the maximum variation of the TD at the site on both days on which SAR image acquisitions were made. The changes in the coordinates corresponding to inclusion or not of meteorological constraints are shown in Fig. 5 and in Figure A1 for the period 2004–2006. Completing these tests allowed us to calibrate the tropospheric contribution to the GPS data collected all over the network and to correct InSAR data for their troposphere contributions.

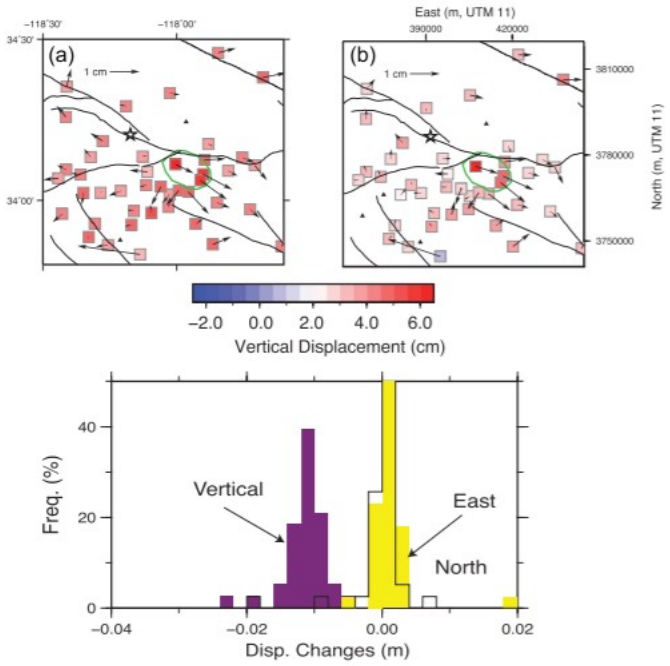

Fig. 5. GPS-measured vertical (color-coded) and horizontal (vectors) displacements between July 20 (day-of-year 201) and January 26 (day-of-year 26) in 2005 for (a) uncorrected and (b) meteocorrected data. The location of the JPLM site is indicated by a star. At JPLM, the troposphere was strongly constrained by the meteorological measurements (P and T) recorded at the surface near the site. We note that the largest horizontal displacements are observed near the maximum uplift location but also close to the edge of a strong troposphere gradient [see Fig. 4(c)] visible on both dates. (c) Histogram of the differences between the uncorrected and corrected displacement components shown in (a) and (b).

SECTION IV.

Results

Fig. 3 shows the troposphere state, as inferred from the measurements of surface temperature, barometric pressure, and relative humidity at meteorological station JPLM (see Figs. 1 and 4) on the dates of the two SAR image acquisitions. Over the interval for which the troposphere estimate is computed (limited by with solid bars), the absolute variation in tropospheric delay is less than 1 cm (see Fig. 4). After the integration of ground meteorological data collected at the site JPLM (see Fig. 3) into the GPS processing, we find, as expected, that the TD estimations vary in time [see Fig. 4(a)], depend on the elevation of the point [see Fig. 4(b)], and are spatially variable [see Fig. 4(c)]. We also still observe, using the available GPS data, a rapid uplift transient in the vicinity of the San Gabriel Valley in the early months of 2005, in agreement with a previous study [62]. We show for reference the coordinate time series of the site CVHS in Figure A1. Using the position on January 26, 2005 as a reference level, we can observe a maximum vertical displacement of ~40 mm in late June 2005. The repeatability of the GPS time series is ±2.5 mm in the horizontal and ±5 mm in the vertical. The inclusion of meteorological data does not affect the

trends of the coordinate time series; however, a systematic bias is removed from the vertical component. The GPS time series can be compared with the displacements imaged by the SAR interferogram in the San Gabriel Valley. We calculate differences in GPS positions at the times of the pre- and postdeformation SAR acquisitions. Those are consistent with up to 4 cm of range decrease in the radar LOS, which is marginally lower than the peak displacement observed in the interferogram (see Fig. 5).

Similarly, we can use the TD estimates obtained from our GPS data to estimate the proportion of the InSAR signal which is due to variations in the troposphere state. In our processing chain, troposphere state is estimated at 2-h intervals, using a 4-h window of data. We believe that this approach is valid as the troposphere state appears stable (i.e., dT~±2 K, dP~1 mbar, dH±~10%) in this area over such a time span (see Fig. 3). Since we sample only the troposphere located above the GPS antenna, we do not need to include the phase variation related to elevation [see Fig. 4(b)] because it is already included in the GPS phase measurements (i.e., the TDs that we estimate are smaller at higher elevations as the signal has traveled a shorter distance through the troposphere).

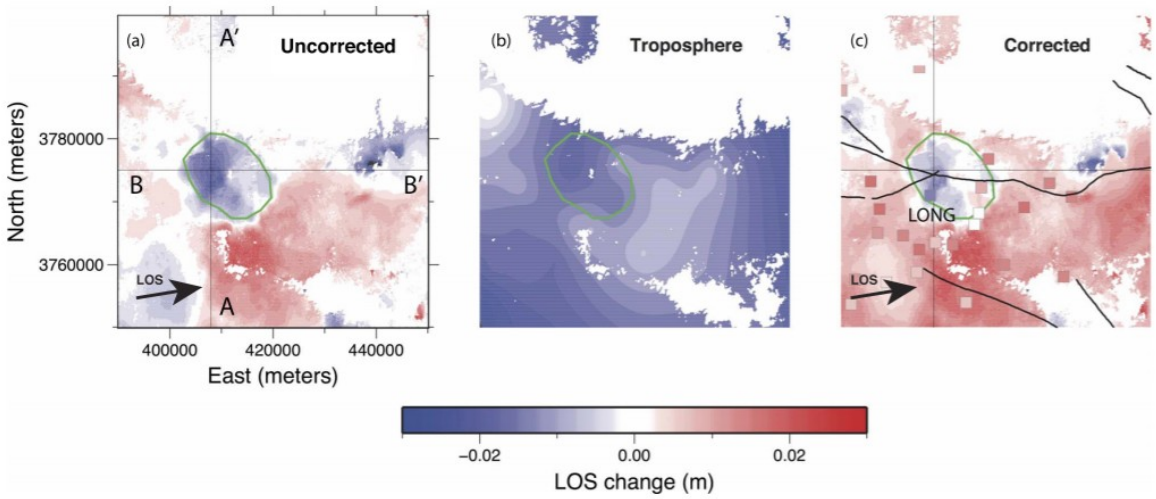

Fig. 6. Example of SAR troposphere correction. (a) InSAR observables (unwrapped phase and converted to displacement) of the area between January 26 and July 20, 2005. (b) Interpolated troposphere model estimated from the GPS ZTD measurements after reprojection into the InSAR LOS. The spatial interpolation assumes an exponential variogram with an e-folding wavelength of 15 km. (c) Residual (corrected) InSAR displacement. The uplift feature close to the GPS site LONG is reduced by ~1.5 cm. This change implies that the peak apparent uplift visible in (a) is related to tropospheric state changes and not to an aquifer expansion. The corrected InSAR displacement field is less variable; the standard deviation of the InSAR interferogram drops from 1.31 to 0.64 cm after application of the troposphere correction. We plot, using squares, the troposphere-corrected GPS vertical displacement presented in Fig. 5(c).

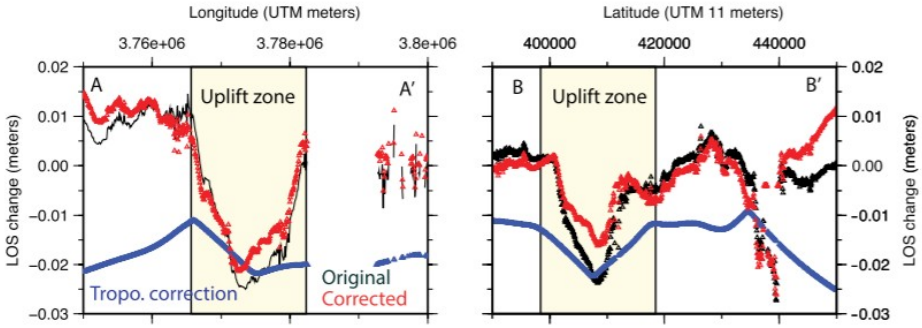

Fig. 7. Comparison of the original (black) and the corrected (red) interferograms along two cross sections shown in Fig. 6. For reference, the TD model used is shown using a blue line. The original and corrected interferograms have been aligned to check if the correction applied was not distorting the displacement profiles in the far field.

For each date, 1) we spatially interpolate ZTD values computed from the combination of the GPS and meteorological data onto a grid with the same pixel spacing as the InSAR data; 2) we project each grid into the LOS direction (i.e., $u'=u/\cos(\theta_{LOS})$, where θ_{LOS} is the incidence angle for the radar signal) specific to each SAR satellite (~23° for the satellite and track used here); and finally, 3) we make the difference between the two grids corresponding to each interferometric pair of SAR images to obtain the difference between the two troposphere states and apply this as a correction to the interferograms. A uniform Kriging algorithm [77] is used for the spatial interpolation, assuming an exponential variogram with an e-folding wavelength of 15 km, which is appropriate given the spacing of GPS sites. An important point to note here is that this interpolation wavelength may not always reflect the length scale of the tropospheric noise in the interferogram. Although it is possible to estimate the variogram of the noise in the interferogram, e.g., by averaging its autocorrelation function [78], in cases where the e-folding wavelength of the noise is shorter than the mean station spacing, any interpolation using that shorter wavelength will only be applicable within that distance from each GPS station; thus, in such cases, we prefer to use an e-folding wavelength longer than the GPS station spacing, with the caveat that the correction will be most effective at longer wavelengths. After projecting the ZTDs onto the LOS vector specific to each SAR satellite, we apply this correction to a 40 km × 50 km portion of the interferogram containing the uplift signal and the central portion of the GPS sites modeled [see Fig. 6(a)]. The troposphere map exhibits a localized signal centered over the GPS site LONG, which is located at the center of the area undergoing uplift. The apparent uplift signal in the SAR interferogram at this location [see Fig. 6(b)] may not, therefore, be exclusively related to a hydrogeological uplift. This TD, appropriately scaled to reflect SAR acquisition geometry, is subtracted from the original InSAR data [see Fig. 6(c)]. We find that the peak of the San Gabriel Valley uplift is reduced by approximately half of one phase cycle (around 15 mm in the satellite LOS) following the application of our correction. The uplift signal appears flatter, with approximately constant range change of 40 mm over an area ~10 km

across. In addition, the local contrast between the uplift and neighboring areas of relative subsidence (e.g., the area immediately to the SE) is reduced.

We additionally tested our approach on other InSAR data (ERS-2 and Envisat) from other tracks available for the same area, which were processed as described earlier (see Figures A2–A11 in supplementary materials). All of the ERS-2 and Envisat data, including both ascending and descending tracks, show similar deformation patterns in space and time, suggesting that the interferograms are primarily recording the uplift of the San Gabriel Valley and that most of that uplift occurred during the period spanning January to May 2005. On some of the images (ERS-2 track 442, January–March 2005; ERS-2 track 170, March–July 2005), the uplifted areas are highlighted only after the troposphere correction is applied, showing similar surface displacement patterns. In general, we find that the areas that were not affected by the uplift are not changed after the troposphere models are implemented (see Fig. 7 and Figures A2–A11). Corrections applied to the InSAR images lie within ±3 cm (1σ interval) with a mean at −0.54±2.6 cm.

The reduction of the uplift observed over the GPS site LONG and the flattening of the signal, in general, to a “plateau” rather than a central “peak” has implications for hydrological models of the San Gabriel aquifer [62]. Specifically, model parameters, such as the aquifer geometry and storage capacity, will be affected. Here, we explore the consequences for those changes to a model previously published [62].

Surface uplift U_z is linked to the water level Δh and the storage coefficient of the medium S_k [79], i.e.,

$$U_z = S_k \Delta h \qquad (7)$$

where Δh is the measured elevation of the water in the wells, and S_k is the storage coefficient. S_k is obviously a parameter that is difficult to assess, but a value on the order of 0.0035 is realistic for a confined aquifer [80], [81]. Since the well elevation level is tightly constrained by observations, the only parameter that could have been impacted is S_k.

The storage coefficient is itself a function of the aquifer structure and of the surrounding rheological settings, such as the thickness of the aquifer b and the specific yield S_y, accounting for the changes in saturation due to the movement of the water table, i.e.,

$$S_k = bS_s + Sy. \qquad (8)$$

S_s can be decomposed itself as

$$S_s = \rho_f g(\alpha + n\beta) \qquad (9)$$

where S_s is a function of the fluid density ρ_f, the uniaxial compressibility of the porous medium α, the compressibility of the fluid β, the porosity n, and the gravitational acceleration g. For this simple treatment, since we do not have any way to demonstrate that S_y is equal to zero, we have chosen, like previous authors [62], to neglect this parameter.

The misestimation of the uplift U_z at the top of the aquifer can thus be interpreted as a change of thickness of the aquifer layer, or a storage coefficient variation. We estimate, based on (7) and (8), that a 15-mm change would lead to an overestimate of the storage coefficient S_k of about ~30% or a change in the aquifer thickness b of the same percentage if saturation is unchanged (dSy/dt). It is difficult to estimate the potential implied change in porosity because porosity is itself pressure/depth dependent. This model fits with the generic model presented before [62]: in which the aquifer is totally flat.

SECTION V.

Discussion and Conclusion

Our test case, as presented earlier, has shown that subtracting out the differential tropospheric delay estimates made with GPS data leads to a "cleaner" interferogram. In cases where the tropospheric signal is overprinted upon a surface deformation signal, it is clear that partial or total masking or anomalous enhancement of such deformation signals may occur. For the 2005 aquifer uplift event in the San Gabriel Valley, the removal of modeled troposphere flattens the peak uplift signal and reduces its peak amplitude. The flattened deformation signal thus obtained leads in turn to a simpler model of the causative aquifer, without need for lateral variations in its storage coefficient. The incorporation of surface meteorological data into our GPS analysis is also demonstrated to have a beneficial effect, allowing to correct for a systematic bias in vertical coordinates and improving the repeatability of coordinate estimates.

The correction proposed here is a first-order correction that may improve the processing of InSAR data by correcting the troposphere contribution in quasi-real time. Obviously, this approach is only possible in areas served by dense networks of C-GPS sites (e.g., California and Japan), although through initiatives such as the PBO under the EarthScope project, density of telemetered C-GPS stations is ever improving; indeed, Fig. 1 shows how the network in the study area has been densified by the addition of PBO stations since 2005. Where the coverage is sufficient, it is not a great computational challenge to implement this type of analysis. A large data volume is not required (a 30-s sampling for GPS data is sufficient), and the analysis can be run episodically (in this case, every 2 h), rather than continuously. In addition, the observation times of the major SAR satellites are known in advance, and thus, additional models can be scheduled automatically to cover those times. Another feature of our strategy is that, if a dense network is not available, the TD mapping and interpolation parameters can be

adjusted to the current network density. Since most of the networks dedicated to the measuring of continental deformation have an intersite distance of ~30–50 km, in such configuration, our strategy would still be able to provide continuous static TD corrections at a given location, albeit at degraded resolution.

Given the impact of troposphere corrections to GPS coordinate time series that results from the inclusion of meteorological data from a single site, an open question is whether further improvements across the network may be possible if such additional data were available at other sites. One could envisage the widespread installation of meteorological sensors at C-GPS stations as already observed for seismic instruments installed in insulated vaults. Campaign GPS measurements may also potentially benefit from temporary deployments of portable sensors during observation epochs. At the time of writing, meteorological data are increasingly, like some types of GPS data, available in real time (from seconds to minutes after observations). The methodology presented in the study allows for the computation of TD maps in real time at a sampling interval of less than 2 h.

ACKNOWLEDGMENT

The authors would like to thank Dr. G. Bawden for the useful early discussions. All Envisat ASAR data are copyrighted by the European Space Agency and were acquired through the WInSAR consortium. Some of the figures were made using the public domain Generic Mapping Tools [82].

N. Houlié had the initial idea and performed the GPS analysis and troposphere modeling. G. J. Funning performed the InSAR analysis and troposphere delay interpolation. All authors participated in the research design and writing.

REFERENCES

1. M. Sneed, M. Ikehara, S. Stork, F. Amelung, D. Galloway, Detection and measurement of land subsidence using interferometric synthetic aperture radar and global positioning system San Bernardino County Mojave Desert California, 2003.

2. T. Burbey, S. Warner, G. Blewitt, J. Bell, E. Hill, "Three-dimensional deformation and strain induced by municipal pumping part 1: Analysis of field data", J. Hydrol., vol. 319, pp. 123-142, 2006.

3. J. W. Bell, F. Amelung, A. Ferretti, M. Bianchi, F. Novali, "Permanent scatterer InSAR reveals seasonal and long-term aquifer-system response to groundwater pumping and artificial recharge", Water Resour. Res., vol. 44, no. 2, Feb. 2008.

4. B. Riedel, A. Walther, "InSAR processing for the recognition of landslides", Adv. Geosci., vol. 14, pp. 189-194, 2008.

5. Y. Yin, W. Zheng, Y. Liu, J. Zhang, X. Li, "Integration of GPS with InSAR to monitoring of the Jiaju landslide in Sichuan China", Landslides, vol. 7, pp. 359-365, 2010.

6. R. Xiao, X. He, "GPS and InSAR time series analysis: Deformation monitoring application in a hydraulic engineering resettlement zone Southwest China", Math. Prob. Eng., vol. 2013, 2013.

7. W. Zhu et al., "Landslide monitoring by combining of CR-InSAR and GPS techniques", Adv. Space Res., vol. 53, pp. 430-439, 2014.

8. P. Cervelli, P. Segall, K. Johnsson, M. Lisowski, A. Miklius, "Sudden aseismic fault slip on the south flank of Kilauea volcano", Nature, vol. 415, pp. 1014-1018, 2002.

9. D. Dzurisin, "A comprehensive approach to monitoring volcano deformation as a window on the eruption cycle", Rev. Geophys., vol. 41, no. 1, pp. 1-29, Mar. 2003.

10. A. Bonforte, A. Carnazzo, S. Gambino, "A multidisciplinary study of an active fault crossing urban areas: The Trecastagni Fault at Mt. Etna (Italy)", J. Volc. Geotherm. Res., vol. 251, pp. 41-49, 2013.

11. S. Metzger, S. Jonsson, G. Danielsen, "Present kinematics of the Tjornes Fracture Zone North Iceland from campaign and continuous GPS measurements", Geophys. J. Int., vol. 192, pp. 441-455, 2013.

12. M. Shirzaei, R. Bürgmann, J. Foster, "Aseismic deformation across the Hilina fault system Hawaii revealed by wavelet analysis of InSAR and GPS time series", Earth Planet. Sci. Let., vol. 376, pp. 12-19, 2013.

13. S. Metzger, S. Jonsson, "Plate boundary deformation in North Iceland during 1992–2009 revealed by InSAR time-series analysis and GPS", Tectonophysics, vol. 634, pp. 127-138, 2014.

14. F. Sigmundsson, A. Hooper, S. Hreinsdottir, "Segmented lateral dyke growth in a rifting event at Bardarbunga volcanic system Iceland", Nature, vol. 517, pp. 191-195, Jan. 2015.

15. G. W. Bawden, W. Thatcher, R. S. Stein, K. W. Hudnut, G. Peltzer, "Tectonic contraction across Los Angeles after removal of groundwater pumping effects", Nature, vol. 412, pp. 812-815, 2001.

16. D. F. Argus, M. B. Heflin, G. Peltzer, F. Crampé, F. H. Webb, "Interseismic strain accumulation and anthropogenic motion in metropolitan Los Angeles", J. Geophys. Res., vol. 110, no. B4, Apr. 2005.

17. R. Bürgmann, G. Hilley, A. Ferretti, F. F. Novali, "Resolving vertical tectonics in the San Francisco Bay Area from GPS and Permanent Scatterer InSAR analysis", Geology, vol. 34, pp. 221-224, 2006.

18. G. Funning, R. Bürgmann, A. Ferretti, F. Novali, A. Fumagalli, "Creep on the Rodgers Creek fault northern San Francisco Bay area from a 10 year PS-InSAR dataset", Geophys. Res. Lett., vol. 34, no. 19, Oct. 2007.

19. R. Jolivet, R. Bürgmann, N. Houlié, "Geodetic exploration of the elastic properties across and within the northern San Andreas Fault zone", Earth Planet. Sci. Lett., vol. 288, pp. 126-131, 2009.

20. N. Houlié, B. Romanowicz, "Asymmetric deformation across the San Francisco Bay Area faults from GPS observations in Northern California", Phys. Earth Planet. Inter., vol. 184, pp. 143-153, 2011.

21. I. Ryder, B. Parsons, T. Wright, G. Funning, "Post-seismic motion following the 1997 Manyi (Tibet) earthquake: InSAR observations and modelling", Geophys. J. Int., vol. 169, no. 3, pp. 1009-1027, Jun. 2007.

22. D. Bekaert, R. Walters, T. Wright, A. Hooper, P. D. J., "Statistical comparison of InSAR tropospheric correction techniques", Remote Sens. Environ., vol. 170, pp. 40-47, Dec. 2015.

23. R. Jolivet, R. Grandin, C. Lasserre, M.-P. Doin, G. Peltzer, "Systematic InSAR tropospheric phase delay corrections from global meteorological reanalysis data", Geophys. Res. Lett., vol. 38, no. 17, Sep. 2011.

24. T. J. Wright, B. E. Parsons, E. J. Fielding, "Measurement of interseismic strain accumulation across the North Anatolian Fault by satellite radar interferometry", Geophys. Res. Lett., vol. 28, pp. 2117-2120, 2001.

25. G. Peltzer, F. Crampé, S. Hensley, P. Rosen, "Transient strain accumulation and fault interaction in the Eastern California shear zone", Geology, vol. 29, pp. 975-978, 2001.

26. E. Tymofyeyeva, Y. Fialko, "Mitigation of atmospheric phase delays in InSAR data with application to the eastern California shear zone", J. Geophys. Res., vol. 120, pp. 5952-5963, 2015.

27. A. Ferretti, C. Prati, F. Rocca, "Permanent scatterers in SAR interferometry", IEEE Trans. Geosci. Remote Sens., vol. 39, no. 1, pp. 8-20, Jan. 2001.

28. P. Berardino, G. Fornaro, R. Lanari, E. Sansosti, "A new algorithm for surface deformation monitoring based on small baseline differential SAR interferograms", IEEE Trans. Geosci. Remote Sens., vol. 40, no. 11, pp. 2375-2383, Nov. 2002.

29. D. A. Schmidt, R. Bürgmann, "Time-dependent land uplift and subsidence in the Santa Clara valley California from a large interferometric synthetic aperture radar data set", J. Geophys. Res., vol. 108, 2003.

30. A. Hooper, H. Zebker, P. Segall, B. Kampes, "A new method for measuring deformation on volcanoes and other natural terrains using InSAR persistent scatterers", Geophys. Res. Lett., vol. 31, 2004.

31. H. Baby, P. Golé, A. Lavergnat, J. A., "Model for tropospheric excess path length of radio waves from surface meteorological measurements", Radio Sci., vol. 22, pp. 1023-1038, 1988.

32. M. Bevis et al., "GPS meteorology: Remote sensing of atmospheric water vapor using the global positioning system", J. Geophys. Res., vol. 97, no. D14, pp. 15 787-15 801, Oct. 1992.

33. M. Bevis et al., "GPS meteorology: Mapping zenith wet delays onto precipitable water", J. Appl. Meteorol., vol. 33, no. 3, pp. 379-386, Mar. 1994.

34. M. Bevis, S. Chiswell, S. Businger, T. T. Herring, Y. Bock, "Estimating wet delays using numerical weather analyses and predictions", Radio Sci., vol. 31, no. 3, pp. 477-487, May/Jun. 1996.

35. C. Rocken et al., "Sensing atmospheric water vapor with the global positioning system", Geophys. Res. Lett., vol. 20, no. 23, pp. 2631-2634, Dec. 1993.

36. C. Rocken et al., "GPS/STORM—GPS sensing of atmospheric water vapor for meteorology", J. Atmos. Ocean. Tech., vol. 12, pp. 468-478, 1995.

37. C. Rocken, T. Van Hove, R. Ware, "Near real-time GPS sensing of atmospheric water vapor", Geophys. Res. Lett., vol. 24, pp. 3221-3224, 1997.

38. F. Brunner, W. Welsch, "Effect of the troposphere on GPS measurements", GPS World, vol. 4, no. 1, pp. 42-51, Jan. 1993.

39. A. Coster et al., "The Westford water vapor experiment: Accuracy issues involving the use of GPS to measure total precipitable water vapor", Proc. 10th Symp. Meteorol. Observ. Instrum. 78th Annu. Meet. Amer. Meteorol. Soc., pp. J70-J75, 1998.

40. G. Ruffini et al., "Estimation of tropospheric zenith delay and gradients over the Madrid area using GPS and WVR data", Geophys. Res. Lett., vol. 26, pp. 447-450, 1999.

41. T. Pany, P. Pesec, G. Stangl, "Atmospheric GPS slant path delays and ray tracing through numerical weather models a comparison", Phys. Chem. Earth A, vol. 26, pp. 183-188, 2001.

42. P. Webley, R. Bingley, A. Dodson, "Atmospheric water vapour correction to InSAR surface motion measurements on mountains: Results from a dense GPS network on Mount Etna", Phys. Chem. Earth, vol. 27, pp. 363-370, 2002.

43. G. Wadge, P. Webley, I. James, "Atmospheric models GPS and InSAR measurements of the tropospheric water vapour field over Mount Etna", Geophys. Res. Lett., vol. 29, 2002.

44. F. Onn, A. Zebker, "Correction for interferometric synthetic aperture radar atmospheric phase artifacts using time series of zenith wet delay observations from a GPS network", J. Geophys. Res., vol. 111, no. B9, Sep. 2006.

45. R. Hanssen, M. Weckwerth, T., H. Zebker, R. Klees, "High-resolution water vapor mapping from interferometric radar measurements", Science, vol. 283, no. 5406, pp. 1297-1299, Feb. 1999.

46. Y. Lin, M. Simons, E. Hetland, P. Muse, C. DiCaprio, "A multiscale approach to estimating topographically correlated propagation delays in radar interferograms", G-Cube, vol. 11, no. 9, Sep. 2010.

47. H. Zebker, P. Rosen, S. Hensley, "Atmospheric effects in interferometric synthetic aperture radar surface deformation and topographic maps", J. Geophys. Res., vol. 102, pp. 7547-7563, 1997.

48. P. Mateus, G. Nico, J. Catalao, "Can spaceborne SAR interferometry be used to study the temporal evolution of PWV?", Atmos. Res., vol. 119, pp. 70-80, 2013.

49. M.-P. Doin, C. Lasserre, P. He, J. De Sigoyer, A. Replumaz, "Multi-temporal InSAR measurement of interseimic motion on the eastern Tibet border", Proc. Fringe Workshop ESA Special Pub., pp. 124, 2015.

50. J. Foster, B. Brooks, T. Cherubini, "Mitigating atmospheric noise for InSAR using a high resolution weather model", Geophys. Res. Lett., vol. 33, no. 16, Aug. 2006.

51. M. Doin, C. Lasserre, G. Peltzer, O. Cavalie, C. Doubre, "Corrections of stratified tropospheric delays in SAR interferometry: Validation with global atmospheric models", J. Appl. Geophys., vol. 69, pp. 35-50, 2009.

52. Q.-M. Chen, S.-L. Song, W.-Y. Zhu, "An analysis of the accuracy of zenith tropospheric delay calculated from ECMWF/NCEP data over Asian area", Chinese J. Geophys.-Chinese Ed., vol. 55, pp. 1541-1548, 2012.

53. Y. Kinoshita, M. Furuya, T. Hobiger, R. Ichikawa, "Are numerical weather model outputs helpful to reduce tropospheric delay signals in InSAR data?", J. Geodesy, vol. 87, pp. 267-277, 2013.

54. R. Jolivet, P. S. Agram, N. Y. Lin, "Improving InSAR geodesy using Global Atmospheric Models", J. Geophys. Res., vol. 119, pp. 2324-2341, 2014.

55. L. Chang, S. Jin, X. He, "Assessment of InSAR atmospheric correction using both MODIS near-infrared and infrared water vapor products", IEEE Trans. Geosci. Remote Sens., vol. 52, no. 9, pp. 5726-5735, Sep. 2014.

56. W.-B. Xu et al., "Correcting atmospheric effects in ASAR interferogram with MERIS integrated water vapor data", Chinese J. Geophys.-Chinese Ed., vol. 53, pp. 1073-1084, 2010.

57. P. Mateus, G. Nico, J. Catalao, "Interpolating MERIS and GPS measurements of precipitable water vapour (PWV) to estimate atmospheric phase delay maps", Proc. Remote Sens. Clouds Atmos., pp. 1-9, 2010.

58. Z. Li et al., "Correcting atmospheric effects on InSAR with MERIS water vapour data and elevation-dependent interpolation model", Geophys. J. Int., vol. 189, pp. 898-910, 2012.

59. S. Williams, Y. Bock, P. Fang, "Integrated satellite interferometry: Tropospheric noise GPS estimates and implications for interferometric synthetic aperture radar products", J. Geophys. Res., vol. 103, pp. 27 051-27 067, 1998.

60. R. Hanssen, Radar Interferometry: Data Interpretation and Error Analysis, Dordrecht, Netherlands:Academic, 2001.

61. Z. Li, E. Fielding, P. Cross, J.-P. Muller, "Interferometric synthetic aperture radar atmospheric correction: GPS topography-dependent turbulence model", J. Geophys. Res., vol. 111, no. B2, Feb. 2006.

62. N. E. King et al., "Space geodetic observation of expansion of the San Gabriel Valley California aquifer system during heavy rainfall in winter 2004–2005", J. Geophys. Res., vol. 112, no. B3, Mar. 2007.

63. P. A. Rosen, S. Hensley, G. Peltzer, M. Simons, "Updated Repeat Orbit Interferometry package released", Eos Trans. Amer. Geophys. Union, vol. 85, pp. 35, 2004.

64. T. G. Farr et al., "The shuttle radar topography mission", Rev. Geophys., vol. 45, 2007.

65. P. Marinkovic, Y. Larsen, "On resolving the local oscillator drift induced phase ramps in ASAR and ERS1/2 interferometric data—The final solution", Proc. Fringe Workshop ESA Special Pub., pp. 124, 2015.

66. R. Scharroo, P. Visser, "Precise orbit determination and gravity field improvement for the ERS satellites", J. Geophys. Res., vol. 103, pp. 8 113-8 127, 1998.

67. R. M. Goldstein, C. L. Werner, "Radar interferogram filtering for geophysical applications", Geophys. Res. Lett., vol. 25, pp. 4 035-4 038, 1998.

68. P. A. Rosen et al., "Synthetic aperture radar interferometry", Proc. IEEE, vol. 88, no. 3, pp. 333-382, Mar. 2000.

69. F. Beauducel, P. Briole, J. Froger, "Volcano wide fringes in ERS synthetic aperture radar interferograms of Etna (1992–1998): Deformation or tropospheric effect?", J. Geophys. Res., vol. 105, no. B7, pp. 16 391-16 402, Jul. 2000.

70. L. Jin, Improving slow ground motion detection using InSAR by applying atmospheric noise mitigation strategies, 2011.

71. N. Houlié, J. Woessner, D. Giardini, M. Rothacher, "Lithosphere strain rate and stress field orientations across the Alpine front", GJI.

72. R. King, Y. Bock, Documentation of the GAMIT Software, 2006, [online] Available: .

73. Z. Altamimi, P. Sillard, C. Boucher, "ITRF2000: A new release of the International Terrestrial Reference Frame for earth science applications", J. Geophys. Res., vol. 107, pp. 2114, 2002.

74. J. Saastamoinen, Atmosphere Correction for the Troposphere in Radio Ranging AOF Satellites, Washington, DC, USA:Amer. Geophys. Union, vol. 15, 1972.

75. L. Essen, K. Froome, "The refractive indices and dielectric constants of air and its principal constituents at 24000 Mc/s", Proc. Phys. Soc., vol. 64, no. 10, pp. 862-875, 1951.

76. J. Triplet, C. Roche, Météororologie Générale, Paris, France:Météofrance, 1983.

77. E. J. Pebesma, C. G. Wesseling, "Gstat: A program for geostatistical modelling prediction and simulation", Comput. Geosci., vol. 24, no. 1, pp. 17-31, Jan. 1998.

78. R. Hanssen, Radar Interferometry, Berlin, Germany:Springer-Verlag, vol. 2, 2001.

79. C. E. Jacob, "On the flow of water in an elastic artesian aquifer", Eos Trans. Amer. Geophys. Union, vol. 2, pp. 574-586, 1940.

80. D. Todd, Groundwater Hydrology, New York, NY, USA:Wiley, 1980.

81. P. Domenico, M. Mifflin, "Water from low-permeability sediments and land subsidence", Water Resources Res., vol. 1, pp. 563-576, 1965.

82. P. Wessel, W. H. F. Smith, "New improved version of generic mapping tools released", Eos Trans. Amer. Geophys. Union, vol. 79, pp. 579, 1998.